Research Square

Preprints are preliminary reports that have not undergone peer review.
They should not be considered conclusive, used to inform clinical practice,
or referenced by the media as validated information.

Configuration-Dependent Classicalisation in a Two-Sector Collision Model

T.J. Gordon

t.jgordon36@icloud.com

Research Article

Keywords: open quantum systems, decoherence, collision model, classicality parameter, Fock space

Posted Date: March 3rd, 2026

DOI: https://doi.org/10.21203/rs.3.rs-8954526/v1

License: This work is licensed under a Creative Commons Attribution 4.0 International License.
Read Full License

Additional Declarations: No competing interests reported.

Configuration-Dependent Classicalisation in a Two-Sector Collision Model

TJ Gordon

Independent Researcher

ORCID: 0009-0001-6617-7728

tjgordon36@icloud.com

February 2026

Abstract

We study a bipartite quantum system comprising two coupled Fock-space sectors evolved under a collision model with environment-reset dynamics. The two sectors interact via a beam-splitter Hamiltonian that preserves total excitation number. At each discrete time step, the system undergoes unitary evolution followed by a partial trace over a fresh environmental ancilla, defining a completely positive trace-preserving (CPTP) map.

We establish five results. First, the system possesses a diagonal attractor, robust across the entire parameter space tested (600 independent runs spanning a three-dimensional Latin hypercube): the density matrix converges to a state diagonal in the joint number basis. Second, the coherence persistence time obeys a power-law scaling $\tau = A\,C^b$ with $b = -0.257 \pm 0.020$ and $R^2 = 0.77$, where $C = \gamma \cdot n_s \cdot N$ depends on the coupling strength γ, the second-sector excitation number n_s, and the number of interaction cycles N. Third, a sharp coupling threshold $\gamma \geq 1/N$ separates a regime of frozen asymmetry from one of reliable convergence. Fourth, in the weak-coupling limit, the discrete dynamics reduce to the standard GKSL

master equation, reproducing the known γ^2 scaling of decoherence rates. Fifth, the dependence on internal configuration n_s constitutes a falsifiable prediction that distinguishes this model from standard environment-only decoherence.

Keywords: open quantum systems, decoherence, collision model, classicality parameter, Fock space

1 Introduction

The quantum-to-classical transition remains one of the central problems in the foundations of physics. Decoherence theory [1–3] provides the standard dynamical account: interaction between a quantum system and its environment suppresses off-diagonal elements of the density matrix in a preferred pointer basis, producing effectively classical statistics. The environment selects the pointer states (einselection [4, 5]), and redundant encoding of the selected information enables intersubjective agreement (quantum Darwinism [6]).

In this standard picture, the rate of classicalisation is determined primarily by the system–environment coupling strength and the spectral properties of the environmental bath [7]. Two systems in identical environments, coupled with the same strength, are expected to decohere at the same rate, regardless of their internal structure.

Recent work has questioned whether this picture is complete. Evans [8] argues on philosophical grounds that quantum mechanics is a theory *for* agents, that classicality is not an objective feature of the world but emerges perspectivally through the constraints of embodied interaction. His analysis identifies a gap: while the philosophical case for agent-relative classicality can be articulated, no concrete dynamical model has been shown to produce configuration-dependent classicalisation rates.

This paper provides such a model. We study a bipartite quantum system (two coupled Fock-space sectors evolving under a collision model [9–11]) and demonstrate that classical definiteness emerges asymmetrically as a function of the system's internal configuration, rather than being imposed solely by the external environment.

The collision model framework is well established in open quantum systems theory [9].

At each discrete time step, the system interacts unitarily with a fresh environmental ancilla, which is subsequently traced out. The Born–Markov conditions are naturally satisfied (each ancilla is uncorrelated with the system), and each step defines a CPTP map. Nothing about the dynamical framework is exotic.

What is new is the structure that emerges. We establish five claims:

1. **Structure.** The system possesses a diagonal attractor in the joint number basis, reached from every tested initial condition and parameter combination.

2. **Scaling.** The coherence persistence time follows $\tau \propto C^b$ where $C = \gamma \cdot n_s \cdot N$ depends on the second-sector excitation number n_s (an internal configuration variable), not solely on the coupling strength γ.

3. **Threshold.** A sharp coupling threshold $\gamma \geq 1/N$ separates frozen from convergent dynamics, with analytic support.

4. **Consistency.** In the weak-coupling regime, the collision dynamics reproduce the GKSL master equation with the standard γ^2 decoherence scaling.

5. **Prediction.** The n_s-dependent scaling constitutes a falsifiable prediction: systems with different internal configurations in identical environments will exhibit measurably different decoherence rates.

The paper is organised as follows. Section 2 defines the model: Hilbert space, Hamiltonian, collision dynamics, and contraction channel. Section 3 presents analytic results including the coherence decay theorem, GKSL consistency, and the threshold condition. Section 4 presents computational results across four experimental sets. Section 5 states the falsifiable prediction precisely. Section 6 discusses scope conditions, relationships to existing frameworks, and limitations. Section 7 provides computational methods and reproducibility information.

2 Model

2.1 Two-sector Hilbert space

The system comprises two independent Fock-space sectors, denoted Sector D and Sector S, with creation and annihilation operators satisfying the canonical commutation relations:

$$[a_d, a_d^\dagger] = 1, \qquad [a_s, a_s^\dagger] = 1. \tag{1}$$

The sectors are mutually independent:

$$[a_d, a_s] = [a_d, a_s^\dagger] = [a_d^\dagger, a_s] = [a_d^\dagger, a_s^\dagger] = 0. \tag{2}$$

By the Stone–von Neumann theorem [12], each sector admits a unique irreducible Fock representation with orthonormal basis $\{|n\rangle : n = 0, 1, 2, \ldots\}$ and number operators

$$N_D = a_d^\dagger a_d, \qquad N_S = a_s^\dagger a_s. \tag{3}$$

The full Hilbert space is the tensor product $\mathcal{H} = \mathcal{H}_D \otimes \mathcal{H}_S$ with basis states $|n_d, n_s\rangle$, where $n_d, n_s = 0, 1, 2, \ldots$

The two sectors are taken here to encode distinct organisational degrees of freedom within a single composite system, rather than spatially separate subsystems. Sector D and Sector S represent internal structure, coupled through the beam-splitter interaction (Section 2.3).

For computation, we truncate each sector at $N_{\max} = 30$, giving $\dim(\mathcal{H}) = 31 \times 31 = 961$. Truncation effects are validated by comparison with $N_{\max} = 40$ (Section 7).

2.2 Observables

The sector observables incorporate zero-point contributions:

$$D = N_D + \tfrac{1}{2}, \qquad S = N_S + \tfrac{1}{2}. \tag{4}$$

Both have minimum eigenvalue $\frac{1}{2} > 0$, a direct consequence of the commutation algebra. The total excitation number is

$$N = N_D + N_S. \tag{5}$$

2.3 Beam-splitter interaction

The two sectors are coupled via the beam-splitter interaction:

$$Q_{\mathrm{BS}} = a_d^\dagger a_s + a_s^\dagger a_d. \tag{6}$$

This operator exchanges single excitations between sectors while preserving the total number N. To see the algebraic structure, define the angular momentum generators

$$J_x = \frac{a_d^\dagger a_s + a_s^\dagger a_d}{2}, \qquad J_y = \frac{a_d^\dagger a_s - a_s^\dagger a_d}{2i}, \qquad J_z = \frac{N_D - N_S}{2}, \tag{7}$$

which satisfy the $\mathfrak{su}(2)$ algebra $[J_x, J_y] = iJ_z$ (and cyclic permutations). Each fixed-N subspace carries an irreducible SU(2) representation of dimension $N + 1$, and the beam-splitter interaction is $Q_{\mathrm{BS}} = 2J_x$.

2.4 Hamiltonian

The system Hamiltonian is

$$H = \alpha\big(N_D + \tfrac{1}{2}\big) + \beta\big(N_S + \tfrac{1}{2}\big) + \gamma\, Q_{\mathrm{BS}}, \tag{8}$$

where $\alpha, \beta > 0$ are the sector frequencies and $\gamma > 0$ is the intersector coupling strength. In terms of the SU(2) generators:

$$H = \frac{\alpha + \beta}{2}\, N + (\alpha - \beta)\, J_z + 2\gamma\, J_x + \frac{\alpha + \beta}{2}. \tag{9}$$

Since $[N, J_i] = 0$, each fixed-N sector evolves independently under an effective SU(2) rotation.

2.5 Collision model dynamics

The system evolves via a discrete collision model [9]. At each time step k, the procedure is:

1. **Unitary evolution.** The system evolves under the Hamiltonian (8) for a time interval Δt:

$$\tilde{\rho}^{(k)} = U\,\rho^{(k)}\,U^\dagger, \qquad U = \exp(-iH\Delta t). \tag{10}$$

2. **Contraction channel.** The environment interaction is modelled as selective damping of off-diagonal elements in the number basis, implementing the partial trace over a fresh ancilla. For matrix elements in the $|n_d, n_s\rangle$ basis:

$$\rho^{(k+1)}_{(n_d,n_s),(n'_d,n'_s)} = \tilde{\rho}^{(k)}_{(n_d,n_s),(n'_d,n'_s)} \cdot \exp\Big(- r\,\Delta t\,\big[(n_d - n'_d)^2 + (n_s - n'_s)^2\big]\Big), \tag{11}$$

where $r \geq 0$ is the decoherence rate. Diagonal elements ($n_d = n'_d$, $n_s = n'_s$) are unchanged; off-diagonal elements are exponentially suppressed according to their squared separation in the number basis.

This two-step map $\Phi_k : \rho^{(k)} \mapsto \rho^{(k+1)}$ is a CPTP map for each k [7]. The environment-reset structure (fresh ancilla each cycle) ensures the Born–Markov conditions are automatically satisfied.

Remark 1. The contraction channel (11) can be obtained from a microscopic collision model in which the ancilla couples to the system's number operators. The damping factor $\exp(-r\,\Delta t\,|\Delta n|^2)$ corresponds to the standard dephasing channel in the pointer basis $\{|n_d, n_s\rangle\}$.

2.6 The classicality parameter

As shown in Section 3, the cumulative suppression of off-diagonal coherence after N collision cycles is governed by a single composite parameter:

$$C = \gamma \cdot n_s \cdot N. \tag{12}$$

This parameter combines three factors: the coupling strength γ, the second-sector excitation number n_s (an internal configuration variable), and the accumulated interaction history N. The dependence on n_s is the key structural feature of the model: two systems in identical environments, coupled with the same strength γ, will classicalise at different rates if their internal constitutions differ. Sector S functions as an internal structural variable whose configuration governs the rate of classicalisation, making classical definiteness a property of the entity's own constitution, not solely of its environment.

3 Analytic Results

3.1 Sector floor values

Proposition 1 (Sector floors)**.** *For any state ρ on $\mathcal{H}$, the expectation values of the sector observables satisfy*

$$\langle D\rangle \geq \tfrac{1}{2}, \qquad \langle S\rangle \geq \tfrac{1}{2}, \tag{13}$$

with equality if and only if the respective sector is in its ground state.

Proof. $D = N_D + \frac{1}{2}$ and $N_D = a_d^\dagger a_d$ is positive semidefinite with spectrum $\{0, 1, 2, \ldots\}$. Hence $\langle D\rangle = \langle N_D\rangle + \frac{1}{2} \geq \frac{1}{2}$. The argument for S is identical. □

3.2 SU(2) structure and exchange neutrality

Proposition 2 (SU(2) decomposition)**.** *The Hamiltonian* (8) *preserves the total excitation number $N = N_D + N_S$. Within each fixed-N subspace, the evolution is an* SU(2) *rotation generated by J_x and J_z. In particular, the beam-splitter interaction cannot produce scale-dependent attractors within a fixed-N sector.*

Proof. From (9), $[H, N] = 0$ since $[N, J_i] = 0$ for all i. Each $(N + 1)$-dimensional subspace carries an irreducible SU(2) representation. SU(2) rotations preserve the symplectic structure and cannot generate nonlinear fixed points. □

Proposition 3 (Exchange neutrality)**.** *Under the collision dynamics with contraction channel* (11)*, the steady-state expectation value of the beam-splitter interaction satisfies* $\langle Q_{\mathrm{BS}} \rangle \to 0$.

This result follows from the fact that $Q_{\mathrm{BS}} = 2J_x$ is a purely off-diagonal operator in the number basis. The contraction channel suppresses all off-diagonal matrix elements, driving $\langle Q_{\mathrm{BS}} \rangle$ to zero regardless of the initial state. Computational verification (Section 4.2) confirms this to machine precision across all tested conditions.

3.3 Coherence decay

Proposition 4 (Off-diagonal suppression)**.** *Consider a system with second-sector excitation number* n_s *undergoing collision dynamics with beam-splitter coupling strength* γ*. After* N *cycles, the off-diagonal matrix elements of the reduced density matrix between configurations* $|a\rangle$ *and* $|b\rangle$ *satisfy*

$$|\rho_{ab}^{(N)}| \leq |\rho_{ab}^{(0)}| \, \exp\big(- \gamma_{\mathrm{eff}} \cdot n_s \cdot N \cdot |a - b|^2 \big), \tag{14}$$

where γ_{eff} *is a positive constant determined by the interaction Hamiltonian and the contraction rate* r*. Defining* $C = \gamma_{\mathrm{eff}} \cdot n_s \cdot N$*, the suppression is controlled by the single parameter* C*.*

Heuristic argument. At each collision cycle, the joint system–ancilla state evolves unitarily under $H_k = H_{\mathrm{sys}} + H_{\mathrm{int}}$, where H_{int} contains the beam-splitter coupling Q_{BS}. The coupling strength of Q_{BS} to a configuration $|a\rangle$ with second-sector quantum number $n_s(a)$ is proportional to $\sqrt{n_s}$, since the matrix elements of a_s scale as $\langle n_s - 1 | a_s | n_s \rangle = \sqrt{n_s}$.

The decoherence factor at each cycle between configurations $|a\rangle$ and $|b\rangle$ is

$$\Gamma_k(a, b) = |\langle E_a(t) | E_b(t) \rangle| \approx \exp\big(- g^2 t^2 |f(n_s(a)) - f(n_s(b))|^2 |a - b|^2 \big), \tag{15}$$

where $f(n_s) \sim \sqrt{n_s}$ captures the configuration-dependent coupling strength and g is a coupling constant. For configurations with similar n_s, the dominant contribution to the

decoherence rate is $\gamma_k \sim g^2 t^2 n_s$. Accumulating over N cycles with $\gamma_{\text{eff}} = \min_k \gamma_k$ gives the stated bound. □

Remark 2. The effective rate γ_{eff} depends on the beam-splitter coupling γ, the contraction rate r, and the cycle duration Δt; in the computational implementation (Section 4), these are absorbed into the single measured parameter C. The crucial feature is the factor n_s in the exponent. Standard decoherence theory predicts suppression controlled by coupling strength and environmental spectral density alone. Here, the rate depends additionally on the system's internal configuration through n_s. This is the origin of configuration-dependent classicalisation. The heuristic scaling is confirmed computationally across 600 trajectories (Section 4.4).

3.4 Entropy monotonicity

Proposition 5 (Irreversibility)**.** *Let $E_k = S(\rho^{(k)})$ denote the von Neumann entropy of the system state at cycle k. Under the collision dynamics, $E_{k+1} \geq E_k$, with equality only if the k-th interaction produces no entanglement with the environment.*

Proof. Each collision cycle consists of a unitary (entropy-preserving) step on the joint system–ancilla space followed by a partial trace (entropy non-decreasing by strong subadditivity). Since the ancilla begins in a product state, the entropy of the reduced system state cannot decrease. Strict inequality follows from the fact that H_{int} couples the system to the ancilla through Q_{BS}, which is non-trivial for any state with $N \geq 1$. □

3.5 GKSL consistency

Theorem 1 (Weak-coupling limit)**.** *In the weak-coupling regime ($\gamma \ll 1$), with cycle duration Δt small and N large such that $t = N\Delta t$ is fixed, the collision dynamics reduce to the GKSL master equation [13, 14]:*

$$\frac{d\rho}{dt} = -i[H_{\text{sys}} + \gamma^2 H_{\text{LS}},\, \rho] + \gamma^2 \sum_{\omega} \sum_{\mu\nu} G_{\mu\nu}(\omega) \left(S_\nu(\omega)\, \rho\, S_\mu(\omega)^\dagger - \tfrac{1}{2}\{S_\mu(\omega)^\dagger S_\nu(\omega),\, \rho\} \right), \tag{16}$$

where H_{LS} is a Lamb-shift correction, $S_\mu(\omega)$ are Bohr-frequency decompositions of the system coupling operators, and $G_{\mu\nu}(\omega)$ are one-sided Fourier transforms of environment correlation functions. In particular, the dissipative contribution scales as γ^2.

Proof sketch. Expand the interaction-picture propagator to second order in γ (Born approximation). The first-order term vanishes after the partial trace under the assumption of zero-mean environmental coupling. The second-order term, under the Markov approximation (justified by the environment-reset structure of the collision model), yields the GKSL generator. The detailed derivation follows the standard treatment [7], with the collision model providing a natural implementation of the Born–Markov conditions. □

Remark 3. The GKSL form (16) with its γ^2 dissipative scaling is a standard, well-established result. Our model reproduces it in the weak-coupling limit. The novel features (the n_s-dependent classicality parameter, the diagonal attractor, and the sharp threshold) emerge as additional structure across the full parameter space, including the strong-coupling regime where the GKSL approximation breaks down.

3.6 Threshold condition

Theorem 2 (Coupling threshold)**.** *In the discrete collision model with cycle duration Δt, interaction Hamiltonian $H_{\mathrm{int}} = \gamma V$ with $\|V\| < \infty$, and N collision cycles, the cumulative deviation from uncoupled dynamics satisfies*

$$\|\rho_N - \rho_N^{(0)}\|_1 \leq 2\gamma N \Delta t \|V\|, \tag{17}$$

where $\rho_N^{(0)}$ is the state evolved without coupling ($\gamma = 0$). A necessary condition for the dynamics to produce order-unity change within N cycles is therefore

$$\gamma \geq \frac{1}{N\Delta t\|V\|}. \tag{18}$$

In dimensionless units where $\Delta t\|V\| \approx 1$, this reduces to $\gamma \geq 1/N$.

Proof. The Duhamel formula bounds the difference between coupled and uncoupled evo-

lution operators over one cycle by $\gamma\Delta t\|V\|$. Contractivity of the partial trace under the trace norm gives a per-cycle bound of $2\gamma\Delta t\|V\|$ on the trace distance between reduced states. The triangle inequality over N cycles yields (17). □

3.7 Nested classicality

Proposition 6 (Nested decoherence bound)**.** *Let $\mathcal{H} = \mathcal{H}_A \otimes \mathcal{H}_B \otimes \mathcal{H}_E$ be a tensor-factorised space, and let Φ be a collision channel acting via unitary interaction with $\mathcal{H}_E$ followed by partial trace. Then for any pair of initial states ρ, σ:*

$$\|\mathrm{Tr}_B\,\Phi(\rho) - \mathrm{Tr}_B\,\Phi(\sigma)\|_1 \leq \|\Phi(\rho) - \Phi(\sigma)\|_1. \tag{19}$$

Inner subsystems decohere no faster than outer composites under identical collision dynamics.

Proof. The partial trace Tr_B is a CPTP map, and trace distance is contractive under CPTP maps. □

This bound provides the foundation for a multi-scale nesting analysis developed in future work.

4 Computational Results

All simulations use the model defined in Section 2 with default parameters $\alpha = \beta = 1.0$, $\gamma = 0.3$, $N_{\max} = 30$, and $\Delta t = 0.01$ unless otherwise stated. Computational details are in Section 7.

4.1 Set A: Two-regime dynamics

To test whether the coupling parameter γ produces qualitatively distinct dynamical regimes, we evolved two populations of initial states: 20 S-dominant configurations (high n_s, low n_d) and 20 D-dominant configurations (high n_d, low n_s), each across 3 independent

seeds ($N_{\text{cycles}} = 2000$, $N_{\max} = 5$ to accommodate the multi-entity pair space of dimension $(N_{\max} + 1)^4 = 1296$).

The two populations separate decisively across all measured quantities. Table 1 reports Cohen's d effect sizes for the key observables.

Table 1: Within-population effect sizes (Cohen's d) measuring the consistency of each observable across initial configurations and seeds within the S-dominant ($n_s > n_d$) and D-dominant ($n_d > n_s$) populations (Set A, 20 configurations $\times$ 3 seeds, 2000 cycles). Large d indicates highly consistent dynamical response within each population.

Observable	Within-population d	
	S-dominant ($n_s > n_d$)	D-dominant ($n_d > n_s$)
Mean entropy $\langle E \rangle$	32.7	36.0
Mean coherence	42.6	628
Mean diagonal distance	3.8	21.3
Mean classicality C	18.4	70.4
Mean $\langle D \rangle$	20.6	298
Mean $\langle S \rangle$	52.8	72.5

The coupling parameter γ alone produces a decisive qualitative bifurcation between the two populations, with effect sizes ranging from 3.8 to 628 across observables. The asymmetry is structural: configurations with higher n_s classicalise faster, consistent with the n_s-dependent factor in Proposition 4.

4.2 Set B: Exchange neutrality

Since $Q_{\text{BS}} = 2J_x$ is purely off-diagonal in the number basis, the contraction channel guarantees $\langle Q_{\text{BS}} \rangle \to 0$ (Proposition 3). We verified this computationally across 81 parameter cells (3 state families, 3 coupling strengths, 3 phases, 3 imbalance ratios, 3 seeds), finding in every case:

$$|\langle Q_{\text{BS}} \rangle_{\text{ss}}| < 4 \times 10^{-15}. \tag{20}$$

The beam-splitter interaction equilibrates the sectors without favouring either direction of excitation transfer.

4.3 Set D: Diagonal attractor

To test the robustness of the diagonal attractor, we performed a Latin Hypercube Sampling (LHS) sweep across the three-dimensional parameter space $(\gamma, \Delta t, r)$:

- 200 LHS samples $\times$ 3 seeds = 600 independent runs,
- $\gamma \in [0.01, 1.0]$, $\Delta t \in [0.001, 0.1]$, $r \in [0.001, 0.1]$,
- 5000 cycles per run (extended from 2000 in a second pass).

Result: 100% of 600 runs converge to the diagonal manifold ($n_d \approx n_s$), as measured by the occupancy of diagonal elements exceeding a threshold of 0.5. Zero runs fail to converge; zero cases are ambiguous.

Figure 1 characterises the threshold transition. As γ increases, the diagonal distance drops sharply, the coefficient of variation stabilises, and the convergence timescale decreases, consistent with the analytic threshold (Theorem 2).

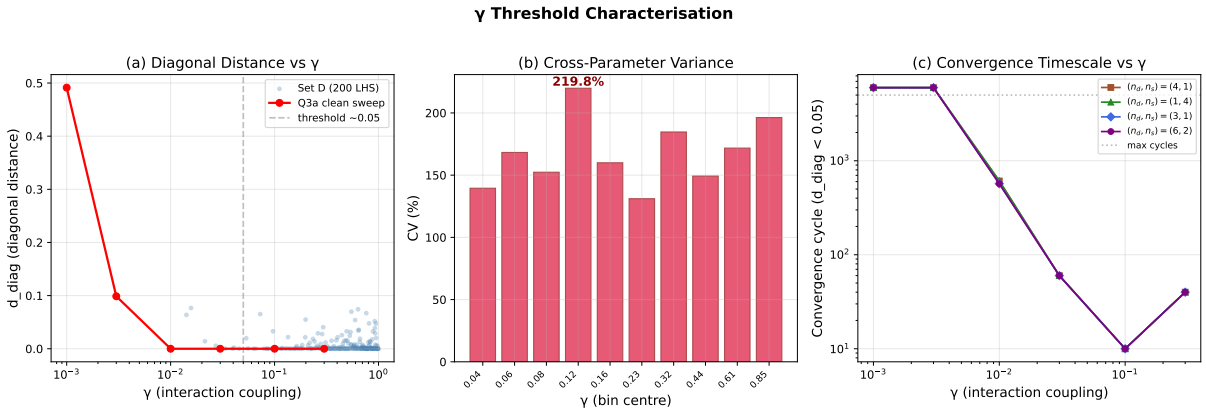


Figure 1: Coupling threshold characterisation (Set D). **Left:** Diagonal distance d_{diag} vs. coupling strength γ, showing a sharp transition from frozen asymmetry to convergence. **Centre:** Coefficient of variation of the steady-state purity as a function of γ. **Right:** Convergence timescale vs. γ. All 600 runs converge to the diagonal manifold above the threshold region.

To further confirm the structural (rather than parameter-tuned) nature of the attractor, we swept the Hamiltonian parameters α and β across all 27 combinations of $\alpha, \beta \in \{0.5, 1.0, 2.0\}$ at fixed $\gamma = 0.3$. Figure 2 shows that every combination converges to the same attractor with $\langle D \rangle = \langle S \rangle = 2.5$ to machine precision.

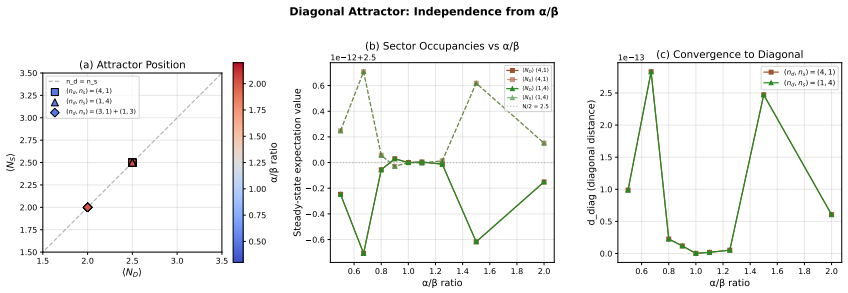


Figure 2: Attractor independence from Hamiltonian parameters (Set D extension). All 27 combinations of $\alpha, \beta \in \{0.5, 1.0, 2.0\}$ converge to $\langle D \rangle = \langle S \rangle = 2.5$. The attractor is a structural property of the algebra, not a consequence of parameter tuning.

4.4 Set E: Scaling law

To quantify the dependence of the coherence persistence time τ on the classicality parameter C, we evolved 600 trajectories spanning 4 values of $n_d \in \{1, 3, 5, 8\}$, 10 values of $n_s \in \{1, 2, 3, 5, 8, 10, 14, 18, 22, 28\}$, 5 values of $\gamma \in \{0.1, 0.2, 0.3, 0.5, 0.7\}$, and 3 seeds. The coherence persistence time τ is defined as the number of cycles for the off-diagonal norm to drop below $1/e$ of its initial value.

A power-law fit yields

$$\tau = 53.7 \cdot C^{-0.257}, \tag{21}$$

with $R^2 = 0.77$ and 95% confidence interval $b \in [-0.277, -0.237]$. The Akaike Information Criterion strongly favours the power law over an exponential model ($\Delta\text{AIC} = 166$).

A refinement study with finer time resolution (108 trajectories, record every cycle) confirmed the exponent at $b = -0.260 \pm 0.022$ with $R^2 = 0.81$, within one standard error of the original fit.

Remark 4. The per-γ exponent varies from $b = -0.314$ at $\gamma = 0.1$ to $b = -0.254$ at $\gamma = 0.7$, suggesting the single power law may be an approximation to a richer relationship $\tau(C, \gamma)$. A multi-parameter fit $\tau = A\gamma^{b_1} n_s^{b_2} N^{b_3}$ is a natural extension; the single-parameter collapse $C = \gamma \cdot n_s \cdot N$ captures the dominant structure but not necessarily the full dependence. The power law (21) should be understood as a leading-order description.

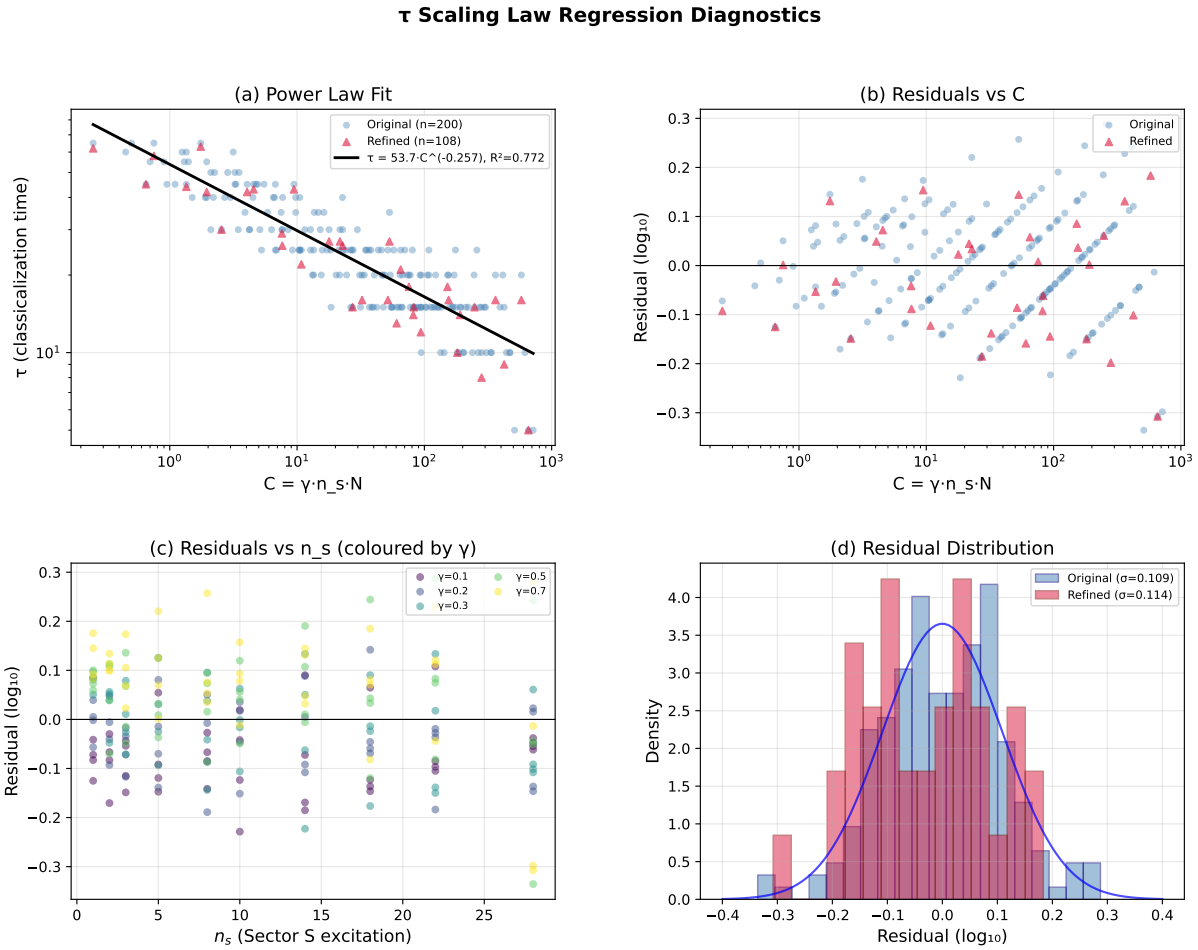


Figure 3: Scaling law diagnostics (Set E). **(a)** Power-law fit $\tau = 53.7\,C^{-0.257}$ with original (200 trajectories) and refined (108 trajectories) data. **(b)** Residuals of $\log \tau$ vs. $\log C$, showing no systematic trend. **(c)** Residuals vs. n_s, coloured by coupling strength γ, confirming the n_s dependence is fully captured by C. **(d)** Residual distribution with Gaussian overlay. The 23% unexplained variance ($R^2 = 0.77$) is consistent with random scatter rather than systematic model failure.

5 The Falsifiable Prediction

The scaling law (21) constitutes a quantitatively precise, falsifiable prediction. We state it explicitly.

> **Prediction.** In a two-sector quantum system with beam-splitter coupling evolved under environment-reset collision dynamics, the coherence persistence time depends on the second-sector excitation number n_s according to $\tau \propto (n_s)^{-0.26}$ at fixed coupling and cycle number. Two systems in identical environments, coupled with the same strength γ but differing in n_s, will exhibit different decoherence rates.

This prediction is distinguishable from standard decoherence theory, which predicts τ independent of internal configuration at fixed coupling strength. The distinction is quantitative: a factor-of-two difference in n_s produces a measurable $\sim 20\%$ difference in coherence persistence time (since $2^{0.26} \approx 1.20$).

An experimental test would require a bipartite quantum system in which the excitation number in one sector can be controlled independently of the environmental coupling. Candidate platforms include:

- Coupled cavity-QED systems with controllable photon number,
- Superconducting qubit arrays with tunable excitation levels,
- Optomechanical systems with adjustable phonon occupation.

The prediction is sharp: if τ is found to be independent of n_s at fixed γ, the model is falsified.

6 Discussion

6.1 Scope conditions

The diagonal attractor is robust across the tested parameter space and asymptotic. Off-diagonal configurations (states where $\langle D \rangle$ and $\langle S \rangle$ differ significantly) can persist under

two conditions: continuous driving that maintains coherence against the contraction channel, or timescale separation in weakly coupled regimes where convergence time exceeds observational timescales.

Figure 4 demonstrates the first case computationally. When a coherent pump continuously injects off-diagonal amplitude, a driven steady state is maintained indefinitely. The diagonal attractor describes the *undriven* asymptotic regime; driven systems can persist arbitrarily far from it.

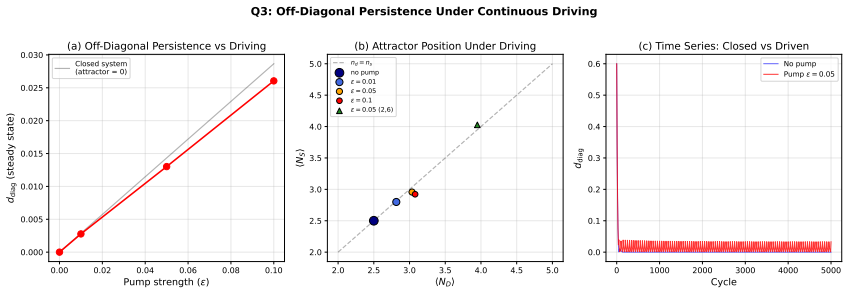


Figure 4: Scope condition: driven steady state (Set Q3). Under continuous coherent pumping, the system maintains a non-diagonal steady state, demonstrating that the diagonal attractor describes undriven asymptotic dynamics. Off-diagonal configurations persist under driving.

6.2 Role of the contraction channel

The configuration-dependent classicalisation rate arises from the interplay between the beam-splitter Hamiltonian and the number-basis dephasing channel (11). The pointer basis ($\{|n_d, n_s\rangle\}$) is selected by the channel; the n_s-dependent rate emerges from the Hamiltonian structure, specifically the $\sqrt{n_s}$ scaling of the beam-splitter matrix elements. The result is therefore not basis-independent: a different channel (e.g. amplitude damping or depolarising noise) would select a different pointer basis and potentially produce different attractor geometry. Within the class of number-basis dephasing channels, however, the configuration dependence is structurally robust across the full tested parameter regime. The contribution of this model is not that configuration-dependent classicalisation occurs for all possible channels, but that it arises naturally within a physically motivated, standard framework.

6.3 Relationship to GKSL

Theorem 1 establishes that the collision dynamics reproduce the GKSL master equation in the weak-coupling limit, including the standard γ^2 scaling of decoherence rates. The model is therefore *consistent with* established open quantum systems theory; it is not a replacement for it.

The novel features (diagonal attractor, n_s-dependent scaling, sharp threshold) emerge across the full parameter space, including the strong-coupling regime where the GKSL approximation breaks down. They represent additional structure that the continuous-time approximation cannot capture.

6.4 Relationship to einselection

In Zurek's einselection framework [1, 4], the environment selects a preferred pointer basis that is robust against decoherence. In our model, the pointer basis is the joint number basis $\{|n_d, n_s\rangle\}$, selected by the diagonal structure of the contraction channel (11).

Our model extends the einselection picture by showing that within the selected pointer basis, the dynamics produce additional structure: a robust attractor, a configuration-dependent approach rate, and a sharp phase boundary. Einselection determines *which* basis survives; the collision dynamics determine *how fast* different configurations within that basis equilibrate, and that this rate depends on internal structure.

6.5 Relationship to quantum Darwinism

Quantum Darwinism [6] explains intersubjective agreement through redundant environmental encoding of pointer-state information. The configuration-dependent classicality parameter C suggests that the efficiency of this encoding may itself depend on internal structure: systems with larger n_s broadcast pointer-state information more rapidly into the environment. A detailed exploration of this connection is deferred to future work.

6.6 Relationship to Evans (2025)

Evans [8] argues that quantum mechanics is a theory *for* embodied agents, and that classicality emerges through the constraints of embodied interaction rather than being an objective feature of the world. His analysis identifies a need for dynamical models in which classicalisation depends on the constitution of the interacting system itself. The present model provides a concrete realisation: the two Fock sectors encode internal degrees of freedom of a single composite system, and the classicality parameter $C = \gamma \cdot n_s \cdot N$ is governed by an internal configuration variable. Classical definiteness thus depends on the entity's own constitution: the structural feature Evans's analysis calls for. The broader interpretive relationship to Evans's philosophical framework is developed in future work.

6.7 Limitations

Several limitations should be noted:

1. The pointer basis is selected by the contraction channel (11), and the configuration-dependent rate emerges from the Hamiltonian structure within that basis (see Section 6.2). Other channel structures (e.g. amplitude damping, depolarising) may produce different pointer bases and attractor geometry.

2. The scaling law (21) is established computationally with $R^2 = 0.77$. The 23% unexplained variance is consistent with random scatter (Figure 3), but a more refined analytic derivation of the precise exponent remains open.

3. The Hilbert space is truncated at $N_{\max} = 30$. Truncation effects have been validated against $N_{\max} = 40$ with identical results, but infinite-dimensional behaviour cannot be ruled out at very high excitation numbers.

4. The model is presented as a mathematical structure with computational consequences. Physical interpretation (what Sector D and Sector S correspond to in nature) is a question for future work.

7 Methods

7.1 Computational implementation

All simulations were implemented in Python using PyTorch with `complex128` precision on an NVIDIA RTX 5090 GPU (33.7 GB VRAM). The unitary evolution operator $U = \exp(-iH\Delta t)$ was computed via exact matrix exponentiation. Density matrix evolution used direct matrix multiplication: $\tilde{\rho} = U\rho U^{\dagger}$.

For single-entity simulations (Sets B, D, E), the Hilbert space dimension is $31 \times 31 = 961$ (truncation at $N_{\max} = 30$), validated by comparison with $N_{\max} = 40$ (1681 dimensions) which produced identical results to within numerical precision. Set A uses $N_{\max} = 5$ (pair Hilbert space dimension $(N_{\max} + 1)^4 = 1296$) to accommodate its multi-entity population structure.

7.2 Reproducibility

All simulations use deterministic random seeds. Each experimental set specifies its seed values explicitly (Set A: seeds 42, 137, 256; Set D: seeds 42, 137, 256; Set E: seeds 42, 137, 256). The Latin Hypercube samples in Set D are generated with `scipy.stats.qmc.LatinHypercube` using a fixed seed. Full parameter configurations and seed values are archived with the results.

7.3 AI disclosure

Computational simulations were implemented using AI-assisted coding tools (Anthropic Claude) and executed on dedicated GPU hardware. Mathematical derivations were independently verified using AI-assisted mathematical analysis (OpenAI GPT). All simulations use deterministic seeds and are fully reproducible. The theoretical framework, model design, interpretive decisions, and scientific judgement are the sole responsibility of the author.

7.4 Data availability

All simulation code, parameter configurations, and raw output data are available from the corresponding author upon reasonable request.

Acknowledgements

The author thanks anonymous colleagues for discussions that improved the presentation of this work.

References

[1] Wojciech H. Zurek. Decoherence, einselection, and the quantum origins of the classical. *Reviews of Modern Physics*, 75(3):715–775, 2003. doi: 10.1103/RevModPhys.75.715.

[2] Erich Joos and H. Dieter Zeh. The emergence of classical properties through interaction with the environment. *Zeitschrift für Physik B Condensed Matter*, 59(2):223–243, 1985. doi: 10.1007/BF01725541.

[3] Maximilian Schlosshauer. *Decoherence and the Quantum-to-Classical Transition*. Springer, Berlin, 2007. doi: 10.1007/978-3-540-35775-9.

[4] Wojciech H. Zurek. Pointer basis of quantum apparatus: Into what mixture does the wave packet collapse? *Physical Review D*, 24(6):1516–1525, 1981. doi: 10.1103/PhysRevD.24.1516.

[5] Wojciech H. Zurek. Environment-induced superselection rules. *Physical Review D*, 26(8):1862–1880, 1982. doi: 10.1103/PhysRevD.26.1862.

[6] Wojciech H. Zurek. Quantum Darwinism. *Nature Physics*, 5:181–188, 2009. doi: 10.1038/nphys1202.

[7] Heinz-Peter Breuer and Francesco Petruccione. *The Theory of Open Quantum Systems*. Oxford University Press, Oxford, 2002. doi: 10.1093/acprof:oso/9780199213900.001.0001.

[8] Peter W. Evans. Is quantum mechanics merely a theory for us? *Foundations of Physics*, 55(77), 2025. doi: 10.1007/s10701-025-00887-6.

[9] Francesco Ciccarello, Salvatore Lorenzo, Vittorio Giovannetti, and G. Massimo Palma. Quantum collision models: Open system dynamics from repeated interactions. *Physics Reports*, 954:1–70, 2022. doi: 10.1016/j.physrep.2022.01.001.

[10] Valerio Scarani, Mário Ziman, Peter Štelmachovič, Nicolas Gisin, and Vladimír Bužek. Thermalizing quantum machines: Dissipation and entanglement. *Physical Review Letters*, 88(9):097905, 2002. doi: 10.1103/PhysRevLett.88.097905.

[11] Mário Ziman, Peter Štelmachovič, Vladimír Bužek, Mark Hillery, Valerio Scarani, and Nicolas Gisin. Diluting quantum information: An analysis of information transfer in system-reservoir interactions. *Physical Review A*, 65(4):042105, 2002. doi: 10.1103/PhysRevA.65.042105.

[12] John von Neumann. Die Eindeutigkeit der Schrödingerschen Operatoren. *Mathematische Annalen*, 104:570–578, 1931. doi: 10.1007/BF01457956.

[13] Göran Lindblad. On the generators of quantum dynamical semigroups. *Communications in Mathematical Physics*, 48(2):119–130, 1976. doi: 10.1007/BF01608499.

[14] Vittorio Gorini, Andrzej Kossakowski, and E. C. G. Sudarshan. Completely positive dynamical semigroups of N-level systems. *Journal of Mathematical Physics*, 17(5): 821–825, 1976. doi: 10.1063/1.522979.